Article

Water-Induced Phase Separation of Spray-Dried Amorphous Solid Dispersions

Na Li, Jonathan L. Cape, Bharat R. Mankani, Dmitry Y. Zemlyanov, Kimberly B. Shepard, Michael M. Morgen, and Lynne S. Taylor*
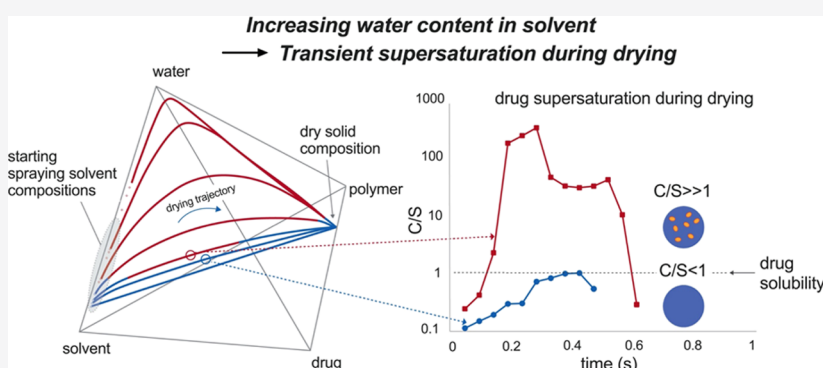
Read Online

ACCESS | Metrics & More | Article Recommendations | Supporting Information

ABSTRACT: Spray drying is widely used in the manufacturing of amorphous solid dispersion (ASD) systems due to its fast drying rate, enabling kinetic trapping of the drug in amorphous form. Spray-drying conditions, such as solvent composition, can have a profound impact on the properties of spray-dried dispersions. In this study, the phase behavior of spray-dried dispersions from methanol and methanol−water mixtures was assessed using ritonavir and copovidone [poly(vinylpyrrolidone-co-vinyl acetate) (PVPVA)] as dispersion components. The resultant ASDs were characterized using differential scanning calorimetry (DSC), fluorescence spectroscopy, X-ray photoelectron spectroscopy (XPS), as well as surface-normalized dissolution rate (SNDR) measurements. Quaternary phase diagrams were calculated using a four-component Flory−Huggins model. It was found that the addition of water to the solvent system can lead to phase separation during the spray-drying process. A 10:90 H_2O/MeOH solvent system caused a minor extent of phase separation. Phase heterogeneity in the 50 and 75% drug loading ASDs prepared from this spray solvent can be detected using DSC but not with other techniques used. The 25% drug loading system did not show phase heterogeneity in solid-state characterization but exhibited a compromised dissolution rate compared to that of the miscible ASD prepared from H_2O-free solvent. This is possibly due to the formation of slow-releasing drug-rich phases upon phase separation. ASDs prepared with a 60:40 H_2O/MeOH solvent mixture showed phase heterogeneity with all analytical methods used. The surface composition of dispersion particles as measured by fluorescence spectroscopy and XPS showed good agreement, suggesting surface drug enrichment of the spray-dried ASD particles prepared from this solvent system. Calculated phase diagrams and drying trajectories were consistent with experimental observations, suggesting that small variations in solvent composition may cause significant changes in ASD phase behavior during drying. These findings should aid in spray-drying process development for ASD manufacturing and can be applied broadly to assess the risk of phase separation for spray-drying systems using mixed organic solvents or other solvent-based processes.

KEYWORDS: amorphous solid dispersions, phase diagram, solvent, spray drying, miscibility

INTRODUCTION

Oral drug delivery is the most prevalent drug delivery route due to its high patient compliance, cost-effectiveness, and ease of dosage form production. For oral formulations, solubilization in aqueous media is a prerequisite for drug absorption. With an increasing number of drug candidates suffering from poor aqueous solubility,[1−3] formulation approaches that enhance solubility and improve bioavailability are being more widely employed. Amorphous solid dispersion (ASD) is one of

the commonly used solubility enhancement strategies, with a high solubility enhancement window and no risk of
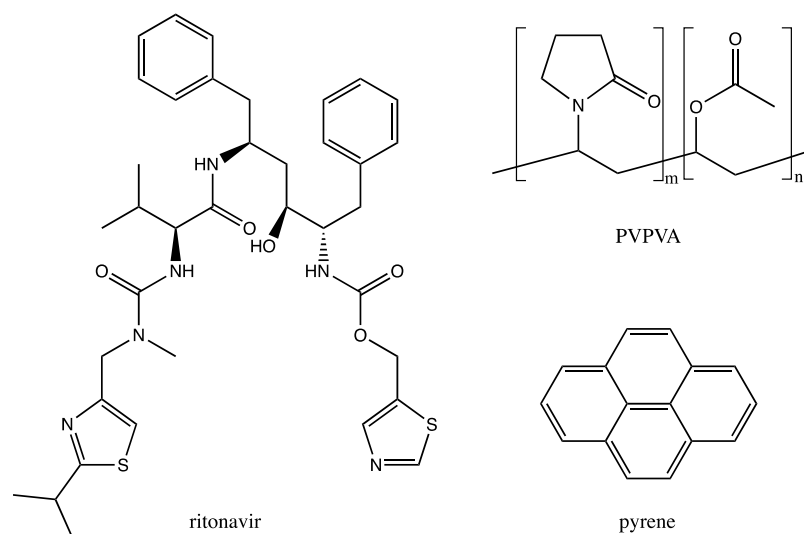
Figure 1. Molecular structures of ritonavir, PVPVA, and pyrene.

compromised permeability compared to other solubilization strategies.[4−7] However, amorphous solid dispersions are kinetically stabilized systems and are prone to phase separation, often driven by the presence of water. Phase separation can occur during manufacturing,[8,9] storage,[10,11] and dissolution[12] of ASDs, resulting in crystallization[13,14] as well as altered drug release,[12,15] and thus leads to compromised product performance. Therefore, being able to detect small extents of phase separation, elucidate the origin of this phenomenon, and understand the impact on ASD performance are all vital for the production of robust formulations.

A variety of analytical techniques has been employed to characterize ASD phase behavior and microstructure. Differential scanning calorimetry (DSC) is usually considered to be the gold-standard method to characterize ASD heterogeneity.[16] However, while the presence of two glass-transition temperatures (T_gs) usually indicates phase separation, a single T_g does not reliably indicate ASD homogeneity.[11] High-resolution imaging-based orthogonal characterization techniques, including atomic force microscopy (AFM) and transmission electron microscopy (TEM), have been recently used in the characterization of ASD phase behavior with high spatial resolution.[15,17−24] These approaches, however, are often limited by the relatively flat (AFM) or thin (TEM) sample requirements for successful implementation of these techniques and are often used for model film samples rather than materials processed using industrially suitable methods, which lead to powder solids. Solid-state nuclear magnetic resonance (ssNMR) spectroscopy is a powerful tool and has been widely used in the characterization of ASD heterogeneity with high spatial resolution;[25−28] nevertheless, the limitation of this technique often lies in the high cost, low sensitivity to small amounts of phase heterogeneity, and long acquisition time. In recent years, fluorescence spectroscopy has been applied to ASD systems to characterize sample homogeneity based on the anisotropy of certain fluorescence dyes and self-fluorescent drugs.[25,29,30] X-ray photoelectron spectroscopy (XPS) has also been used in the surface characterization of spray-dried ASD particles because of its short penetration depth.[9,31,32]

In industrial manufacturing, ASDs are commonly produced via either spray drying or hot-melt extrusion.[33] While hot-melt extrusion is limited to thermally stable drugs with sufficiently

low melting points in combination with low-T_g (glass-transition temperature) polymers, spray drying is commonly used for commercial formulations of drugs soluble in a low-boiling-point solvent.[33] Current investigations on ASD phase behavior are mostly focused on theoretically calculated miscibility,[34−39] as well as model systems prepared via spin-coating,[23] rotary evaporation,[15] film casting,[40,41] or solvent-free techniques.[42−44] For ASDs produced by spray drying, properties have been found to depend on various factors, such as solvent composition,[45,46] solid loading,[46] drying rate,[40] and dryer geometry.[47] However, the mechanisms by which spray-drying parameters alter ASD phase behavior remain obscure. Further, characterization approaches for ASD particles are still evolving. It has been demonstrated that the presence of trace amounts of water in otherwise nonaqueous solvent systems can lead to substantial ASD phase separation during drying via spin-coating and rotary evaporation.[15,23] This could potentially be problematic for spray drying, as water may be present in the spray solvent if the spray solvent is exposed to ambient conditions or added to improve the solubility of certain components. Additionally, solvent mixtures such as methanol and dichloromethane are often used in spray drying to solubilize both the drug and the polymer. Due to differences in boiling point and polarity, a similar risk of ASD phase separation is expected during spray drying when the solvent composition changes.

The goals of the current study were twofold: to understand the impact of a binary solvent system containing water on the miscibility of a model ASD prepared by spray drying, and to develop new experimental and theoretical approaches to track the phase behavior. Ritonavir was selected as a model compound due to its slow crystallization propensity, which enables amorphous phase separation to be evaluated. Copovidone [poly(vinylpyrrolidone-co-vinyl acetate) (PVPVA)] was selected as the model polymer since it is widely used in commercial ASD formulations and is readily soluble in methanol and water. Trace amounts of pyrene were added to the spray solution to enable monitoring of ASD phase behavior following particle formation. The chemical structures of ritonavir, PVPVA, and pyrene are shown in Figure 1. To characterize the phase behavior of the spray-dried ASDs, a combination of different techniques, including DSC, fluo-

rescence spectroscopy, and XPS, was used for orthogonal validation purposes. Surface-normalized dissolution studies were performed to evaluate ASD release performance.

■ MATERIALS AND METHODS

Materials. Ritonavir was purchased from ChemShuttle (Wuxi, China), PVPVA-64 (Kollidon 64) was sourced from BASF (Florham Park, NJ), and pyrene was purchased from Sigma-Aldrich (St. Louis, MO). Methanol and acetonitrile were purchased from Mallinckrodt Baker (Phillipsburg, NJ). All other chemicals were obtained from Sigma-Aldrich (St. Louis, MO). Reverse osmosis water with a resistivity lower than 18 MΩ was used in all experiments.

Methods. *Preparation of Spray-Dried Dispersions (SDDs).* Spray-dried ritonavir−PVPVA dispersions were produced using different H_2O/MeOH ratios. Stock solutions at 25, 50, and 75 wt % drug loadings (relative to total solids) were prepared at a solid loading of 4%. Detailed spray-drying parameters are listed in Table 1. The resultant SDD particles

Table 1. Spray-Drying Parameters

spray-drying parameters	conditions used
spray dryer	BLD-35
inlet temperature	175−195 °C
outlet temperature	50 °C
solid loading	4%
atomization pressure	120 psi
drying airflow	450 g/min
solution feeding rate	25 g/min
nozzle	Schlick 2.0

were secondary dried in a Gruenberg benchtop tray dryer at 30 °C for at least 12 h. The samples were then stored at 4 °C with drierite. Prior to use, the samples were then allowed to equilibrate to room temperature with a desiccant present. A weight percentage (relative to total solids) of 0.1% (well below the solubility limit of pyrene in the ASD) of pyrene was also incorporated in the ASD matrix as a fluorescence marker to characterize ASD homogeneity. The samples prepared at different conditions for various analyses are summarized in Table 2.

Table 2. SDDs Prepared for Characterization Using Various Analytical Approaches

drug loading (%)	solvent composition	analyses
25%, 50%, 75% (with 0.1% pyrene)	100% MeOH, 10:90 H_2O/MeOH, and 60:40 H_2O/MeOH	DSC
		fluorescence spectroscopy
	PXRD	
		SNDR
		XPS
50%	20:80 H_2O/MeOH and 40:60 H_2O/MeOH	DSC

Characterization. Powder X-ray Diffraction (PXRD). Powder X-ray diffractograms of the crystalline drug, physical mixtures of the drug and polymer, as well as spray-dried dispersions were collected using a Rigaku SmartLab diffractometer (Tokyo, Japan). Powder samples were packed onto glass sample holders and analyzed using copper Kα radiation.

Data were collected from 5 to 35° 2θ using a scan rate of 4°/min and a step size of 0.04°. A silicon standard was analyzed prior to sample data collection.

Differential Scanning Calorimetry (DSC). The glass-transition temperature (T_g) of spray-dried dispersions was determined using a Q2000 DSC (TA Instruments, New Castle, DE). Briefly, the samples of 2−5 mg were placed in nonhermetic pans with no pinholes (TA Instruments, New Castle, DE), scanned from 0 to 150 °C at a ramp rate of 2.5 °C/min, with 1.5 °C/modulation and a 60 s period. The midpoint of the glass-transition event was reported as the T_g. The nonhermetic seal allows the solvent to escape upon heating.

Fluorescence Spectroscopy. The fluorescence spectra of both powder solid samples and spin-coated films were collected using an RF-5301PC fluorometer (Shimadzu, Kyoto, Japan). The powdered samples were sandwiched between two quartz slides. A solid sample holder was used to hold the sample slides. The excitation wavelength of 332 nm with an emission wavelength range of 332−550 nm was selected. The excitation and emission slit widths of 5 and 1.5, respectively, and a 0.2 nm scanning interval with an autoresponse time were chosen. All fluorescence spectra were collected at a high sensitivity setting.

X-ray Photoelectron Spectroscopy (XPS). XPS spectra were collected using a Kratos Axis Ultra DLD spectrometer (Kratos Analytical, Manchester, U.K.) with a monochromatic Al Kα radiation (1486.6 eV) at a pass energy of 20 and 160 eV for high resolution and survey spectra, respectively. To achieve better resolution and to avoid nonhomogeneous electric charge of nonconducting powders, a commercial Kratos charge neutralizer was used. Binding energy (BE) scale was calibrated using Au $4f_{7/2}$ at 84.0 eV and Cu $2p_{3/2}$ at 932.67 eV. A double-sided Cu tape was used to place the powder samples on a stainless steel holder.

Data analysis was conducted using CasaXPS (www.casaxps.com). The charge correction was performed by setting the C−C component of the C 1s peak at a BE of 284.8 eV for each sample. The atomic concentrations of each element were calculated after a Shirley background subtraction considering the corresponding Scofield atomic sensitivity factors and the contribution due to different inelastic mean free paths of photoelectrons. The XPS data were averaged over at least four spots spatially separated to avoid possible X-ray damage. The atomic concentrations were then converted to drug concentrations in mass percentage.

Surface-Normalized Dissolution Rate (SNDR) Determination. The surface-normalized dissolution rate of SDDs was carried out using Wood's intrinsic dissolution apparatus (Agilent Technologies, Santa Clara, CA). Briefly, approximately 50 mg of ASD powder was weighed and placed in the die cavity. The punch was then placed in the die (8 mm i.d.) to form a flat surface. Another 50 mg of ethyl cellulose was weighed and placed in the die cavity on top of the ASD layer. This was added as a backing material to fill in the die cavity.[31] Subsequently, the sample was tableted using the punch with a compression pressure of 1500 psi for 2 min. The die containing the sample was then unscrewed from the surface plate and mounted onto a shaft connected to an overhead stirrer (IKA Works Inc., Wilmington, NC). SNDR experiments were carried out with a rotational speed of 100 rpm at pH 6.5 using 100 mL of 50 mM sodium phosphate buffer. Neat

amorphous ritonavir powder was also prepared via rotary evaporation and tableted as a control.

For each sampling point, 0.5 mL of the dissolution media was taken and replenished with fresh media. As matrix disintegration did not occur, these samples were not filtered. The samples were diluted immediately with 50:50 acetonitrile/ water to eliminate the risk of drug crystallization and then further diluted to the desired concentration range for high-performance liquid chromatography (HPLC) analysis. Briefly, an Agilent 1260 Infinity series HPLC (Agilent Technologies, Santa Clara, CA) and a Waters XTerra RP C-18 column (150 mm × 4.6 mm, i.d. 3.5 μm) (Waters Corp., Milford, MA) were used. The mobile phase consisted of 60% acetonitrile and 40% water. Ritonavir was detected at 210 nm with an injection volume of 10 μL and a flow rate of 1 mL/min. The total run length was 7 min. Calibration curves were constructed over the concentration ranges of 0−100 ng/mL, 100−1000 ng/mL, and 10−60 μg/mL. About 6−9 time points were taken for each experiment. The slope of the concentration, normalized by the surface area of the dissolving front of the tablet and the drug loading of the ASD, versus time plot, was used to calculate the surface-normalized dissolution rate. Each experiment was repeated in triplicate.

Particle Size Determination. The particle size of any drug-rich colloids generated during dissolution or upon water addition to the solvent was measured via dynamic light scattering using a Malvern nanoZS Zetasizer (Malvern Instruments, Westborough, MA). Solutions or suspensions were analyzed immediately after sampling to minimize particle growth or agglomeration. Triplicate samples were measured. The viscosity and refractive indices of the dispersant were corrected using previously published data by Thompson et al.[48] and Herráez et al.,[49] or measured using an SV-10 AND vibro viscometer (A&D Company Ltd., Tokyo, Japan) as described previously.[15]

Kinetic and Thermodynamic Modeling. A kinetic model for spherical droplet drying was developed and coupled to thermodynamic calculations of the free-energy surface for the four-component system of methanol, water, ritonavir, and PVPVA. Conservation equations for heat and mass transfer and discretization of the radial coordinate were used to derive a system of ordinary differential equations (ODEs) representing heat and mass fluxes. The droplet and surrounding (spherical) vapor phase were discretized into radially symmetric systems, and the combined condensed and vapor phases were treated as a closed system (see the Supporting Information).

Evaporation at the droplet surface was treated via a modified form of the Maxwell model. Solvent loss and evaporative cooling were related by the latent heat of evaporation. Heat loss cascades radially, as described by ODEs representing linear heat gradients between volume elements. Radial convective mass transfer is simulated via an empirical mass transfer constant between volume elements, which is decoupled from heat transfer to simplify the model. The shrinking droplet boundary was found by recalculating a total volume at each time step. Model outputs are the radial mass composition and temperature as a function of time.

Phase behavior is predicted using a four-component Flory−Huggins model, parameterized by six χ parameters: $\chi_{12}, \chi_{13}, \chi_{14}, \chi_{23}, \chi_{24}, \chi_{34}$, where 1 = methanol, 2 = water, 3 = ritonavir, and 4 = PVPVA. $\chi_{14}, \chi_{23},$ and χ_{24} are calculated from room-temperature dynamic vapor sorption data, χ_{13} was determined

from the measured room-temperature solubility of ritonavir in methanol, χ_{12} was estimated from the reported enthalpy of mixing of methanol and water, and χ_{34} was estimated from the observed ritonavir miscibility in PVPVA in spray-dried dispersions. Based on the wide miscibility of RTV in PVPVA, χ_{34} is likely <0.5 and possibly close to zero. Sensitivity analyses show that χ_{34} impacts the drug−polymer binary line but does not significantly affect phase boundaries crossed early in the drying trajectory. Drying kinetics and free-energy surfaces were calculated using the numerical integration platform Berkeley Madonna v. 8.0.1, using the Euler integration algorithm, with a time step of 1 ms and a total integration time of 1 s.

Binodal locations in the free-energy surface were calculated by scanning the potential energy surface. Minima in the free-energy curves were located using a minimization algorithm implemented in Microsoft Excel.

RESULTS

Physicochemical Properties. The physicochemical properties of ritonavir and PVPVA are shown in Table 3.

Table 3. Physicochemical Properties of Ritonavir and PVPVA

	ritonavir	PVPVA
molecular weight	720.94	45 000−70 000[50]
log P	5.98[16]	
T_m	128 °C	
T_g	51 °C	108 ± 1 °C[18]
pK_a	1.8 and 2.6[51,52]	
crystalline solubility (pH 6.5, ionic strength 0−100 mM)[53]	1.3−2.4 μg/mL	
amorphous solubility (pH 6.5, ionic strength 0−100 mM)[53]	19−38 μg/mL	

Ritonavir is a weakly basic compound with pK_a values <3, with a negligible extent of ionization at pH 6.5. It has a relatively slow crystallization propensity[16] and therefore is a suitable model compound for miscibility and dissolution evaluations without interference from drug crystallization. It has a glass-transition temperature of 51 °C and an amorphous solubility of 19−38 μg/mL in pH 6.5 buffer with ionic strength from 0 to 100 mM at 37 °C.[53]

PVPVA is a synthetic random copolymer with good solubility in a wide range of polar and nonpolar organic solvents,[50] eliminating the need to use organic solvent mixtures for spray drying. It has a glass-transition temperature of 108 °C.[18] Therefore, in the absence of water, amorphous solid dispersions formed with ritonavir and PVPVA likely existing in the glassy state at room temperature.

Solid-State Characterization. *PXRD and DSC.* Ritonavir SDDs at different drug loadings were analyzed using powder X-ray diffraction and differential scanning calorimetry to assess crystallinity and miscibility, respectively. Representative results are shown in Figures 2 and 3. The lack of sharp peaks in the diffractograms suggested that the SDDs are X-ray amorphous. This is also supported by the lack of a melting peak in the DSC thermograms obtained from the various SDDs.

For SDDs produced from the single solvent system (methanol), a single glass-transition temperature was observed at all drug loadings. Increasing drug loading resulted in a lowered SDD T_g. For SDDs produced from binary solvent
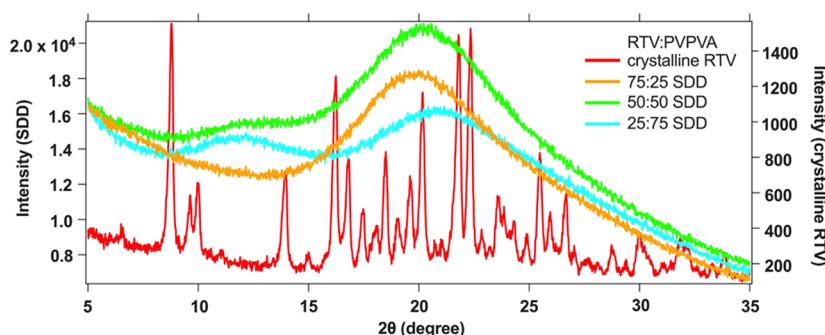
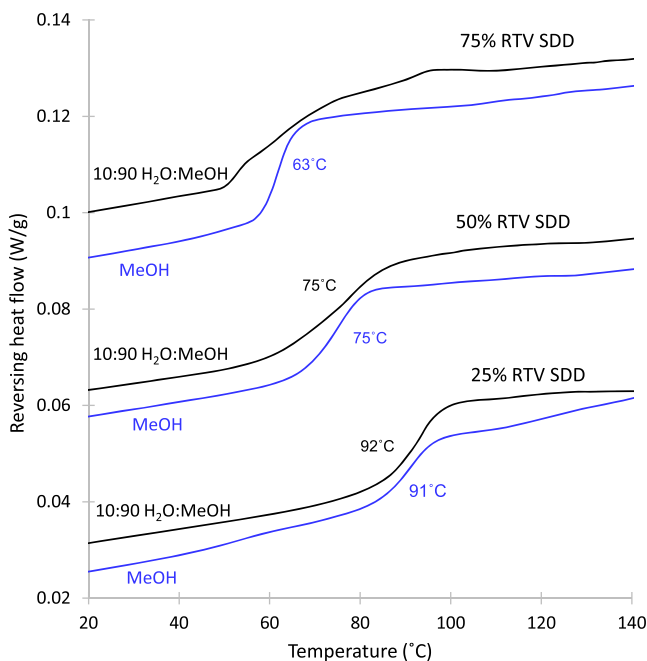**Figure 2.** Powder X-ray diffractogram overlay of crystalline ritonavir and SDDs spray-dried from methanol.

Figure 3. Glass-transition events of RTV: PVPVA SDDs with different drug loadings spray-dried from a MeOH or a 10:90 H_2O/MeOH solvent system.

systems (10:90 w/w H_2O/MeOH), a single T_g was observed at 25 and 50% drug loadings. However, this does not necessarily mean phase homogeneity. The breadth of the glass transition for a 50% loading SDD spray-dried from 10:90 w/w H_2O/MeOH was slightly larger than for the pure methanol case. This may indicate subtle inhomogeneity, and thus, further investigations were carried out as described below. At a 75% drug loading, multiple glass transitions were present, suggesting the formation of multiple amorphous phases in the SDD.

To further interrogate the effect of solvent water content on phase separation, 50% ritonavir SDDs were spray-dried from four solvent mixtures: pure methanol (0:100 w/w H_2O/MeOH), 10:90, 20:80, and 40:60 H_2O/MeOH.

Initial DSC analysis of the four resulting SDDs yielded ambiguous results with broad transitions (data not shown). It was unclear if small bumps in the modulated DSC non-reversing trace were due to small amounts of residual solvent or the enthalpy overshoot of a second glass transition at low temperature. To improve resolution, the samples were aged for 72 h at 40 °C, a sufficiently low temperature to avoid induction of phase separation. If the low-temperature peak decreased in

size, it could be attributed to solvent loss. If the peak remained or increased in size, it could be assigned to the enthalpic signature of the drug-rich phase. Results for SDDs spray-dried from the four solvent systems are shown in Figure 4. The reversing traces demonstrate a gradual broadening of the glass transition with increasing water content, and two clear transitions for the 40:60 H_2O/MeOH solvent system. The nonreversing traces for the 10:90, 20:80, and 40:60 H_2O/MeOH systems contain two distinct peaks, confirming the presence of a second phase.

Fluorescence Spectroscopy. Fluorescence spectroscopy was also used to investigate the phase behavior of ritonavir SDDs prepared at different conditions. Pyrene was selected as a fluorescence sensor as its emission spectrum is sensitive to the local polarity, and it has been utilized to evaluate phase separation previously.[25,29]

Representative pyrene emission spectra are shown in Figure 5, showing its complex five-peak emission spectrum between 370 and 405 nm, as well as the excimer peak at around 460 nm in pyrene crystals, which arises only when two fluorophores are spatially proximal.[54]

In the five-peak emission region, the peak 1/3 ratio changes with the polarity of the environment surrounding pyrene molecules. Typically, a higher peak 1/3 ratio indicates a more polar environment, whereas a lower peak 1/3 ratio corresponds to a less polar environment.[29] For SDDs prepared at different conditions, the pyrene peak 1/3 ratios are plotted as a function of drug loading (Figure 6). It can be seen that for SDDs prepared with methanol, the peak ratios decreased linearly with increasing drug loading, corresponding to the decreasing polarity of the system to the increased amount of the more lipophilic drug. SDDs prepared with 10% water and 90% methanol exhibited nearly identical peak 1/3 ratios compared to SDDs prepared with methanol alone. For SDDs prepared with 60% water and 40% methanol, a significant decrease in peak 1/3 ratio was observed at all three drug loadings, 25, 50, and 75%. Such changes suggest that the local environment surrounding pyrene molecules became less polar. This could be due to the formation of drug-rich regions upon phase separation and the preferential distribution of pyrene with the drug-rich phase. We also induced SDD phase separation by storing originally miscible SDD samples (prepared with methanol alone) at 75% RH. These samples also showed decreases in pyrene peak 1/3 ratios, consistent with phase separation.

X-ray Photoelectron Spectroscopy. The surface composition of the SDD particles was also evaluated using XPS as an orthogonal technique. Drug concentrations were calculated based on curve fitting of the O 1s and C 1s peaks. S 2p peaks
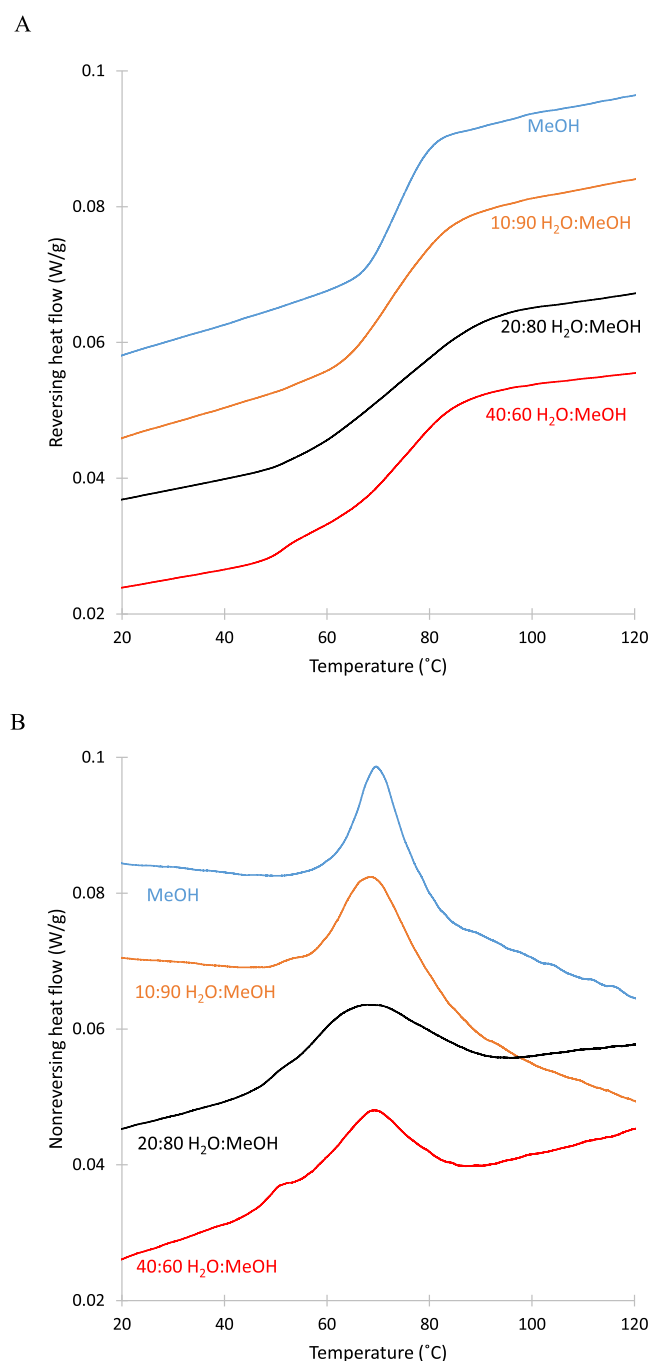
A

B

Figure 4. DSC thermograms of 50% ritonavir−PVPVA SDDs (aged) sprayed from various H$_2$O/methanol mixtures. (A) Reversing heat flow and (B) nonreversing heat flow.

were also used for validation purposes. XPS spectra of the pure compounds were used as model peak shapes for curve fitting. The results are plotted as a function of the nominal drug loading, as shown in Figure 7. Numerical values are also provided in the Supporting Information.

For SDDs prepared from methanol, high linear correlations were observed between the measured surface drug composition and nominal drug loading (R^2s of 0.9720 and 0.9946 for O 1s and C 1s data, respectively). Such results suggested that ritonavir was homogeneously distributed within these SDD particles. For SDDs prepared with 10% water and 90% methanol, slight deviations were observed at 25 and 75% drug

loadings. For samples prepared with 60% water and 40% methanol, significant surface drug enrichment was observed at 25 and 50% drug loadings. For SDDs at a 25% drug loading, the surface composition ranged from 59 to 70% ritonavir, whereas for SDDs of a 50% drug loading, 85−91% drug was found on the surface. For this solvent system, phase separation was observed prior to spray drying, with the formation of drug-rich droplets suspended in solution containing dissolved polymer;[23,55,56] thus, a suspension was spray-dried. The phase heterogeneity in the feed material can be carried over to the spray-dried solids upon drying.[15] Since the composition of each phase is dependent on solvent composition rather than the drug loading of the ASD,[15] it is not surprising that ASDs at different drug loadings sprayed from 60% water and 40% methanol showed similarly high drug contents on the surface (Figure 7B). Also, during spray drying, the drying front moves inward from the particle surface. Since water has a relatively higher boiling point than methanol and thus remains in the particle for a longer period of time, the lower solubility drug may precipitate, causing surface drug enrichment.

Due to the limited penetration depth of pyrene emission light, the solid-state fluorescence technique also appeared to be surface-sensitive. By plotting the pyrene peak 1/3 ratio of miscible SDDs as a function of drug loading (data from Figure 6), a calibration curve can be constructed. The surface composition of SDDs prepared from different solvent systems can then be back-calculated, and the resultant values are plotted with the measured surface composition by XPS (Figure 8). Good agreement was obtained between fluorescence and XPS data.

Dissolution Performance. The dissolution performance of SDDs prepared at different conditions was evaluated using an intrinsic dissolution apparatus to eliminate the impact of particle size variations and matrix disintegration effects. Amorphous ritonavir (100% RTV) was studied as a control. Results of SDDs with various drug loadings produced from different solvent compositions are shown in Figure 9.

For SDDs at a 75% drug loading, the surface-normalized dissolution rates were similar to that of the neat amorphous drug, and spray solvent composition showed no significant effect on dissolution rate. The 50% drug loading system showed slightly higher dissolution rates than that of the neat amorphous drug, but spray solvent composition did not alter dissolution rates of this system significantly. This may also be because the dissolution conditions used in this work were not discriminative for these systems.[57]

For the 25% drug loading system, the highest dissolution rate was observed for SDDs sprayed from methanol alone. Water addition in the spray solvent system, even at a relatively low amount (10%), decreased the surface-normalized dissolution rate by nearly half. A higher amount of water addition (60%) further decreased the dissolution rate of the system to about a quarter of the original value.

Apparently, the addition of water in the solvent system greatly altered the dissolution performance of these SDDs, likely as a result of phase separation. For systems at a 25% drug loading prepared with 60% water, both fluorescence and XPS spectroscopy suggested phase separation and surface drug enrichment. Such surface drug enrichment could prevent or slow down further drug release from the inner core of the particle and thus may lead to a decreased dissolution rate. For the 25% drug loading system prepared with 10% water, no significant change was observed in fluorescence, XPS spectra,
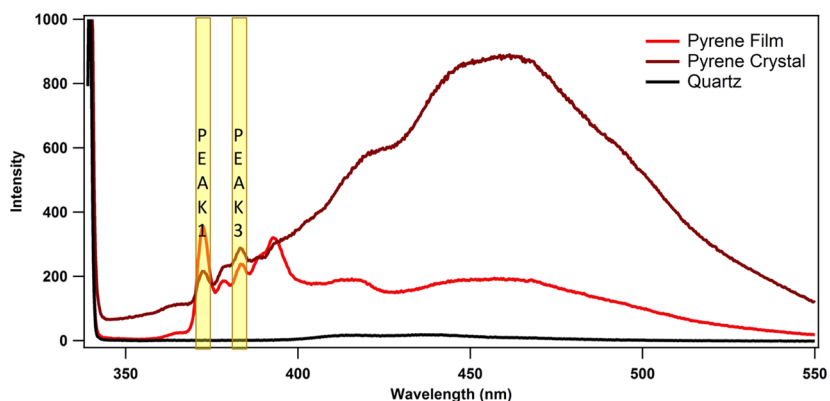
Figure 5. Representative fluorescence spectra of pyrene. The pyrene film was made by spin-coating of 0.1% pyrene dispersed in 20 mg/mL PVPVA methanolic solution onto a quartz slide. Pure crystalline pyrene was sandwiched between two quartz slides. The background signal from the quartz slide is also shown.
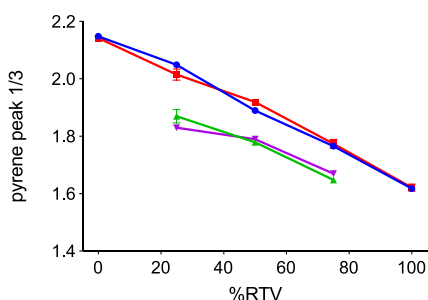

Figure 6. Pyrene peak 1/3 ratios of different SDD samples.
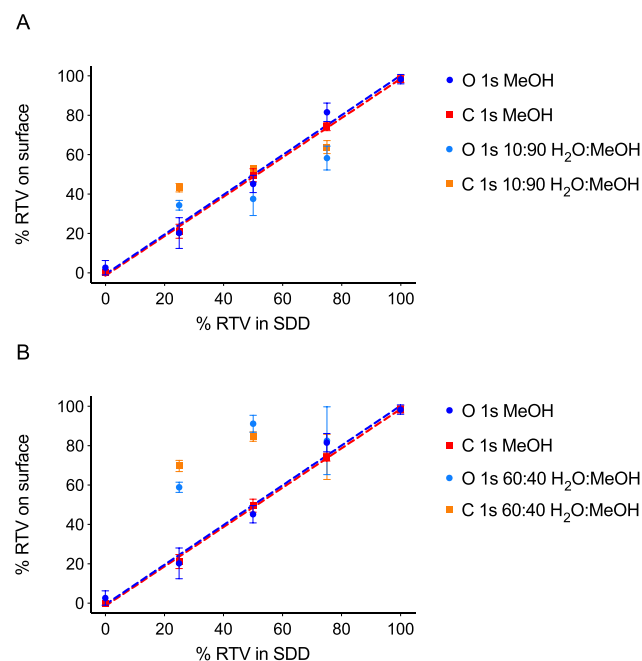

Figure 7. Surface drug distribution in SDDs from XPS analyses (control SDDs prepared from pure methanol showed good linearity with drug loading as shown in blue and red; dashed line: linear regression fitting line using O 1s/blue or C 1s/red data of control SDDs). (A) SDDs spray-dried from H$_2$O/MeOH (10:90 w/w). (B) SDDs spray-dried from H$_2$O/MeOH (60:40 w/w).

Figure 8. Calculated drug concentrations using pyrene peak 1/3 ratio and XPS results (dashed line showing diagonal). (A) Using the O 1s and (B) using the C 1s peaks from the XPS spectra.

Figure 9. Surface-normalized dissolution rates of ritonavir−PVPVA SDDs prepared from different solvent systems (100% amorphous RTV prepared by rotary evaporation).

or DSC thermograms. Although microstructural and local compositional changes may be subtle, they caused remarkable changes in dissolution performance.
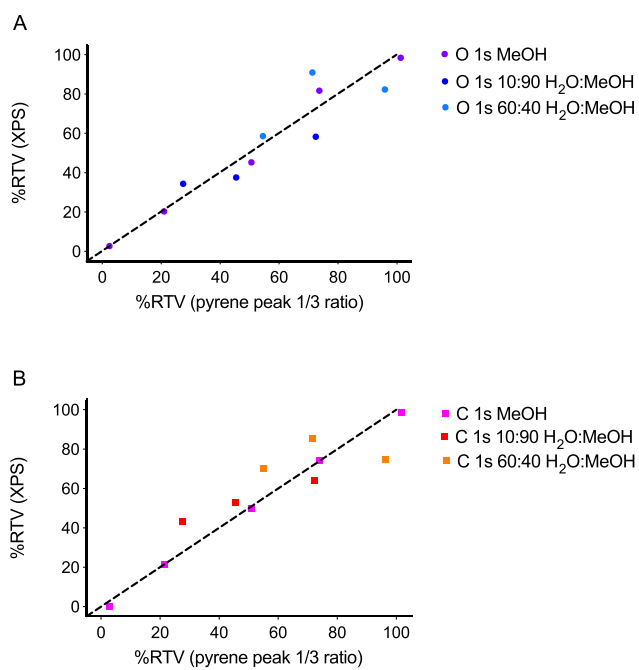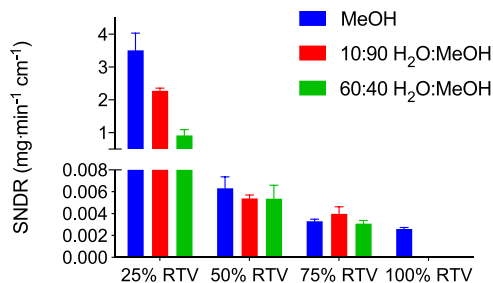
Although solvent-induced phase separation greatly compromised the dissolution performance of SDDs at a 25% drug loading, it is worth noting that the surface-normalized dissolution rates obtained from these systems were still more

than 100 times higher than those of miscible SDDs at 50 and 75% drug loadings (Figures 9 and 10). The drug concentration
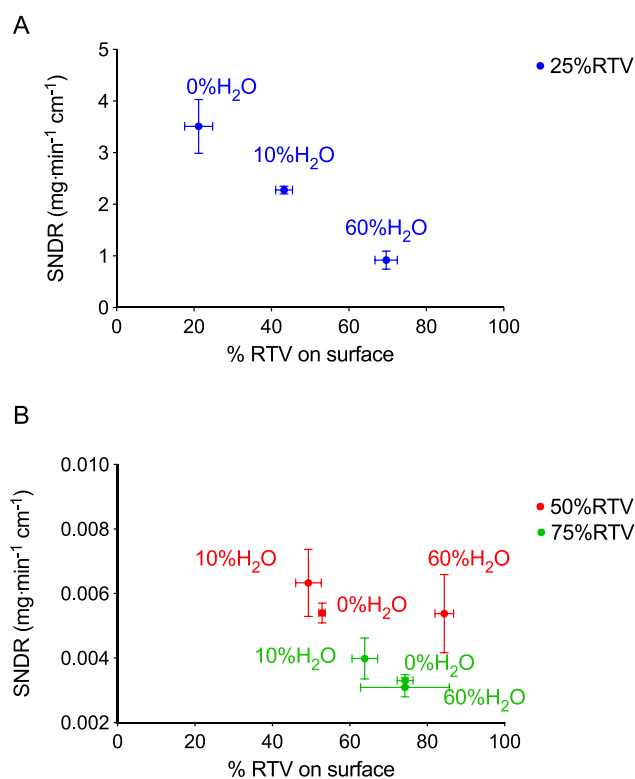

Figure 10. Surface-normalized dissolution rates of ritonavir−PVPVA SDDs as a function of surface drug content as calculated from XPS results. (A) 25% drug loading system. (B) 50 and 75% drug loading systems.

exceeded the amorphous solubility of ritonavir with drug-rich droplets formed during the dissolution of all SDDs at a 25% drug loading, even those showing phase separation.

Drug-rich colloids were not observed for SDDs at higher drug loadings. The size of colloidal species formed in solution during dissolution ranges from 390 to 467 nm, as shown in Table 4, whereas the size of precipitates formed by adding 60

Table 4. Size of Colloidal Species Generated during Dissolution

sample	sampling time (min)	size (nm)
25% drug loading, 100% methanol	60	390 ± 21
25% drug loading, 10:90 H_2O/MeOH	60	467 ± 24
25% drug loading, 60:40 H_2O/MeOH	130	454 ± 23

wt % water to MeOH (i.e., those formed in the 60:40 H_2O/MeOH solvent system with a 1.6% solid content) was measured to be 1626 ± 94 nm. The stock solution used for spray drying had a 4% solid content, and thus, an even larger particle size is expected in the initial suspension. Particles formed upon atomization and spray drying are usually in the micron range unless a special nozzle is used to produce submicron particles. In addition, with soft low-T_g materials such as amorphous drug nanoparticles formed in solution upon liquid−liquid phase separation, spray drying can facilitate particle growth instead of breakage, and therefore, a large

amount of stabilizers such as sugars are needed to maintain particle stability.[58]

Therefore, colloidal species formation during dissolution is not related to the discrete domains formed in the particles because of phase separation induced by the spray solvent composition. Clearly, colloid formation during ASD dissolution is a result of liquid−liquid phase separation upon fast drug release in solution. Although the addition of water to the spray solvent caused phase separation and compromised drug release in ASDs, fast drug release and colloid formation can still be achieved at a 25% drug loading even when 60% water was added to the solvent system.

■ DISCUSSION

ASD Phase Behavior during Spray Drying. Consideration of the water content in the spray solvent is important because in industrial practice, water is sometimes added to the solvent system to help dissolve certain polymers or surfactants during ASD production. Also, although counterintuitive and not applicable for ritonavir studied herein, the addition of water to organic solvent can often increase drug solubility in the spray solvent. Although the stock solution may remain miscible with a small amount of water added, the added water can have a profound impact on the microstructure and dissolution performance of resultant ASDs if phase separation occurs during spray drying. Additionally, if the solvent used in the spray-drying operation is hygroscopic (such as methanol and acetone), it can easily pick up a substantial amount of atmospheric moisture during storage and handling. The results presented herein clearly demonstrate that the presence of water in the spray solvent can lead to phase separation/heterogeneity in the resultant SDD particles.

Solvent mixtures, such as methanol and dichloromethane, are widely used to solubilize cellulose-based polymers in the production of spray-dried ASDs. Since different solvents possess distinct boiling points and heat of vaporization, solvent composition changes are expected during spray drying. If the solubility difference of the drug and the polymer in each solvent is significant, phase separation during the drying trajectory is also possible. Water and methanol used in this study serve as examples of antisolvent and solvent, respectively, for the drug. The polymer, copovidone, has good solubility in both solvents.

To better understand the experimental results, the impact of water in the solvent mixture on the phase behavior was investigated using a heat and mass transport model to simulate compositional trajectories during drying. A Flory−Huggins model was then applied to define the solubility boundaries of ritonavir in these simulations. The calculated phase diagrams are shown in Figures 11 and 12. The two-phase region is represented by the red curves in a series of drying simulations, each of which starts from a different H_2O/MeOH ratio in the solvent fraction. Collectively, these traces map the binodal boundary for ritonavir solubility and allow one to assess phase separation risk from a thermodynamic perspective.

In the absence of water (W), the drug (D), polymer (P), and solvent (S) are completely miscible, and the system is represented by the bottom plane of the tetrahedron, **DPS**. Therefore, rapid solvent removal during spray drying should result in homogeneous ASDs. Moving toward the water apex of the diagram, the drying curves map out a wide two-phase region for the system where the drug concentration exceeds its amorphous solubility. When water is added to the initial
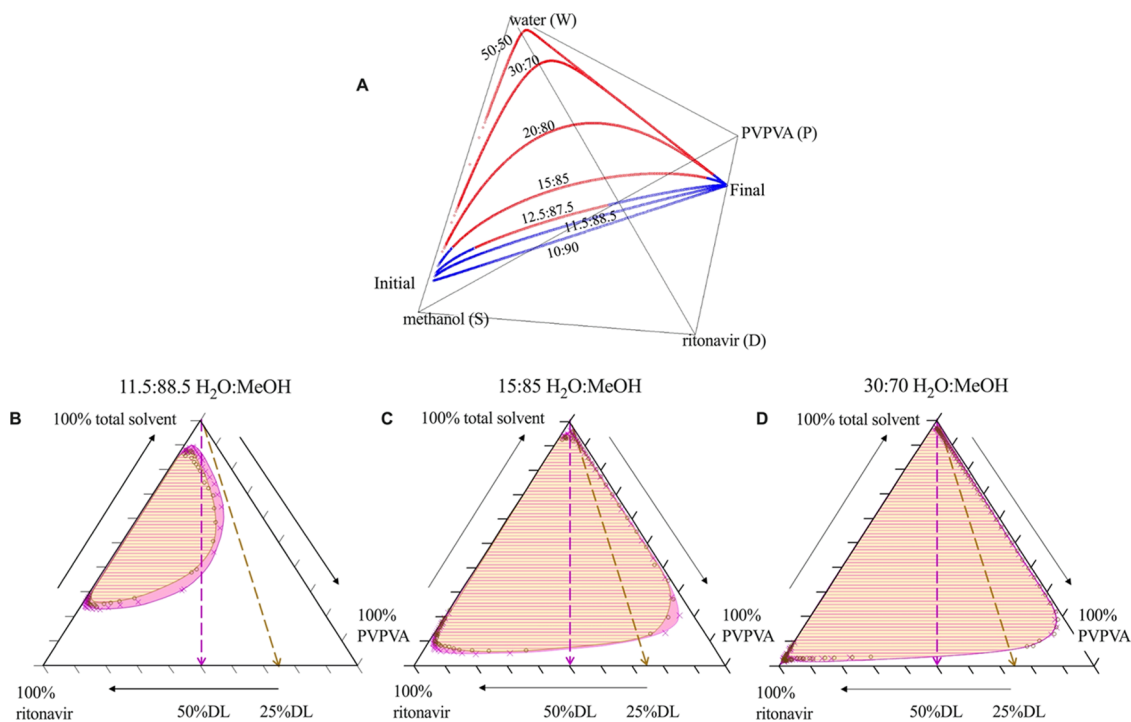
Figure 11. Calculated phase diagrams for the ritonavir−PVPVA−methanol−water system. (A) Predicted compositional trajectories during drying plotted in the quaternary phase space for a 25% drug loading at varying H_2O/MeOH ratios. The blue regions indicate the portions of each trajectory where the drug is below its solubility, and the red regions indicate the drug being above its solubility. Collectively, the red regions map the two-phase region for the 25% drug loading slice of the quaternary space. (B−D) Extracted pseudo-ternary diagrams from this same data set, treating the total solvent (water + methanol) as a single axis. The pink region indicates the mapped two-phase regions at a 50% drug loading (DL), whereas the brown gridded region corresponds to a 25% DL.
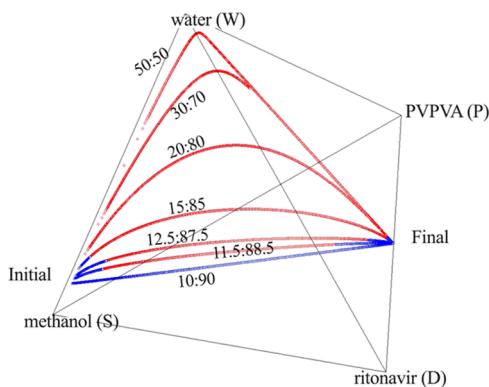

Figure 12. Predicted compositional drying trajectories plotted in the quaternary phase space for a 50% drug loading at varying H_2O/MeOH ratios.

solution, the drying trajectory begins to assume a parabola shape due to the faster evaporation rate of methanol relative to water. At progressively higher water contents, the curved paths of the trajectories cause the composition to move closer to, and eventually through, the two-phase (water-rich) region of the diagram, as shown by the red regions of trajectories in the tetrahedron (Figures 11A and 12). For the specific parameters used in these simulations, the threshold bulk water content, at which the trajectory passes through the two-phase region, is approximately 12.5/87.5 H_2O/MeOH at a 25% drug loading (DL) (Figure 11A), although this may move higher or lower depending on concentration gradients, which were not explicitly considered in these simulations, and the limited accuracy of χ parameters. Eventually, the water is removed

during drying, creating a downward path to the drug/polymer axis in the lower right of the diagram. At the end of each drying trajectory, when the solvent content of the system becomes sufficiently low, the favorable interaction parameter between the drug and polymer components moves the system back into a thermodynamically stable single-phase region. Increasing the water content of the initial spray solution rapidly reduces the drug solubility such that the starting points for the higher water content trajectories begin in a thermodynamic two-phase region. The overlap area between the two-phase region and the drying trajectory encompasses a wider span of compositions of the drying droplet at higher drug loading. For example, the 11.5:88.5 H_2O/MeOH solvent system completely passes through the miscible region at a 25% drug loading (Figure 11A) but is largely phase-separated at a 50% drug loading (Figure 12). These simulations illustrate that a composition starting as a single-phase solution and ending as a miscible binary drug−polymer amorphous dispersion can indeed pass through thermodynamically immiscible regions of the phase diagram. The risk for phase separation depends on how deeply within the two-phase region the drying curve passes, which impacts the degree of supersaturation, as well as the duration spent in this region.

The pseudo-ternary diagrams shown in Figure 11B−D demonstrate the sensitivity of this system to drug loading. These diagrams are two-dimensional representations of the three-dimensional quaternary plot (Figure 11A) and help to further illustrate the impact of drug loading and water content. At low water contents, the drying curves may only graze or can completely bypass the two-phase region. For example, in Figure 11B, at an 11.5/88.5 H_2O/MeOH ratio, drying of the

low-drug-loading (25%) system safely bypasses the two-phase region, whereas, at high drug loading (50%), the trajectory may pass tangentially through the two-phase region. At higher water content (diagrams C and D), the effect of drug loading is less pronounced because all compositions are already spending the bulk of their trajectory in phase-separated space.

The composition of the phase-separated drug-rich phase is also found to depend on the initial water content of the stock solution. Drying trajectories that take the composition deep into the two-phase region show a drug-rich phase consisting almost entirely of drugs due to the larger miscibility gap in this area. Trajectories that only graze the two-phase region may exhibit phase-separated states that are slightly less enriched in drugs and mixed with either the solvent or polymer, depending on whether one is observing phase separation early or late in the drying process. This agrees with our experimental observations shown in Figure 7. SDDs prepared from a 60:40 H_2O/MeOH solvent system have more drug enriched on the surface of particles, where phase separation is present in the spray mixture before the spray-drying step, compared to the 10:90 H_2O/MeOH solvent system. For the 25% drug loading system, both spray solvent compositions resulted in phase-separated ASDs with compromised dissolution performance to various degrees (Figure 9). The 50% drug loading system, on the other hand, shows clear differences in DSC thermograms with different extents of phase separation (Figure 4). Overall, a larger extent of phase separation was observed when more water was added in the spray solvent. This is because the 60:40 H_2O/MeOH system was phase-separated in the spray solvent mixture and has a larger miscibility gap than the 10:90 H_2O/MeOH system.

Although the phase diagrams in Figures 11 and 12 demonstrate at which point during the drying trajectory a particular system will be thermodynamically unstable, they do not make clear the driving force leading to phase separation, which is also available from the output of the simulations. To illustrate this, the degree of supersaturation for two different solvent compositions at a 25% drug loading is shown in Figure 13A. The total water content is also shown in Figure 13B to provide a sense of how the concentration-to-solubility ratio C/S varies with the dynamic water content during drying. These figures represent the interplay of the drug solubility and instantaneous drug concentration responding to the effects of both increasing water (driving C/S up) and increasing polymer (driving C/S down). At intermediate time points, there is a complex interplay between these factors. As the solvent continues to exit the particle, solid loading increases. However, increased polymer content can also facilitate drug solubilization. Near the end of the trajectory, the water content decreases to zero and C/S drops again.

At the 12.5:87.5 H_2O/MeOH ratio, the drug concentration increases just above the C/S = 1 boundary to generate a transient period of supersaturation. The drug concentration for the 15:85 H_2O/MeOH ratio encounters a much wider time frame of supersaturation with over a 100-fold higher driving force for phase separation. Collectively, these simulation results demonstrate that a small increase in the initial water content, when near a phase boundary, can have strong effects on both the driving force and time scale available for phase separation.

Sensitivity of Different Analytical Approaches. DSC is usually the gold-standard technique used in the evaluation of ASD miscibility based on the presence of single or multiple glass-transition events.[59] However, a phase-separated ASD may
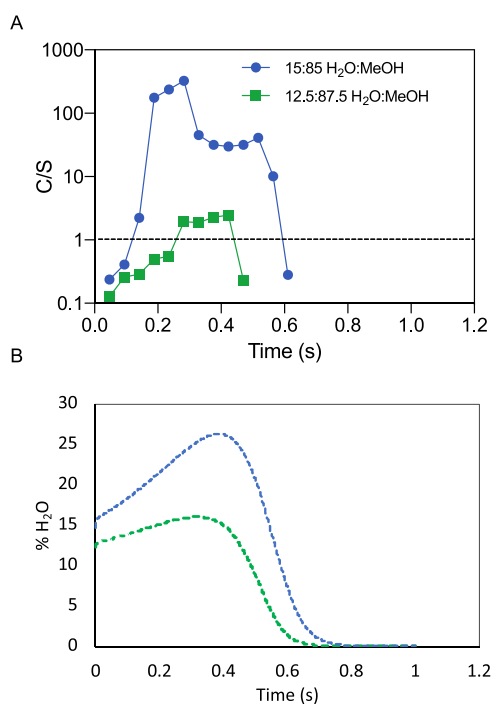

Figure 13. (A) Degree of supersaturation (concentration-to-solubility ratio C/S) and (B) water content throughout the drying time scale extracted from two trajectories with differing starting solvent compositions for a 25% drug loading system.

not always be detected by DSC due to either domain sizes <100 nm or small differences in the T_gs of the pure components.[11,18] On the other hand, in polymer blends, the presence of two T_gs does not necessarily indicate immiscibility.[60−62] In addition, heat-induced mixing or demixing of the drug and polymer may restrict the application of DSC for characterization of ASD miscibility at room temperature.[21] In this study, the modulated DSC with no sample aging was not able to pick up two distinctive T_gs with the exception of a 75% drug loading system prepared with 60% water in solvent (Figure 3). By carefully aging below the onset of sample mobility to allow the pre-existing amorphous phases to age to lower-energy states without changing the microstructure of the system, it was possible to improve the resolution of this technique to confirm phase separation in 50% drug loading systems prepared with 10, 20, and 40% water in solvent (Figure 4). Any pre-existing phase separation can be readily detected as the enthalpic relaxation peak grows. These results highlight the importance of complementary analytical techniques to confirm the thermal analysis findings of nonequilibrium materials such as ASDs.

Fluorescence and X-ray photoelectron spectroscopies have been recently used in the characterization of miscibility in polymer and drug blends.[3,21,29−32,63−65] The peak 1/3 ratio of pyrene was shown to be sensitive to the local environment, specifically the polarity, around the pyrene molecule.[66] This approach possesses a high spatial sensitivity, with the capability of detecting heterogeneous domains of 2−8 nm in an itraconazole−HPMC amorphous solid dispersion system.[25] The sample penetration depth of light is a high-order nonlinear function dependent on wavelength for a given material. For shorter wavelengths in the UV−vis region, the penetration depth can be as little as a quarter of the wavelength of light hitting the sample. Therefore, fluorescence from solids is

usually a surface measurement depending on the particle size. XPS is also a surface-sensitive quantitative technique. Typically, it measures the kinetic energy and number of electrons that escape from the surface of material within 0−10 nm depth. In this study, good agreement in surface composition calculated from fluorescence spectroscopy and XPS was obtained (Figure 7), suggesting the potential of fluorescence spectroscopy to quantitatively assess the surface composition of SDDs as a fast and low-cost method.

The dissolution test was used as an indirect measure of phase separation in this study. For a miscible ASD, the dissolution rate of the poorly soluble drug is dependent on drug loading. For copovidone-based dispersions, it has been noted that at low drug loadings, the polymer controls the drug release rate. In this instance, the polymer and drug release at the same rate, with rates similar to that of the polymer alone, and the release is said to be congruent.[67] When a critical drug loading is exceeded, which varies depending on the drug, the drug release rate reduces dramatically.[67] The congruent release boundary is usually low, with reported values ranging from 5% to about 30% drug loadings.[68−71] The congruent release boundary of ritonavir−PVPVA ASDs was found to occur at a 25% drug loading.[67] At higher drug loadings (40 and 50%), the initially miscible ASDs showed incongruent release of the drug and polymer, with the drug release rate similar to that of the neat amorphous drug.[67] ASD phase separation can alter the dissolution performance in different ways.[3,12,15,72] The mechanisms involved can be multifold, but it was recently suggested that the local composition of phase-separated domains is one of the dominating factors for altered dissolution performance.[15] Phase separation can lead to the formation of drug-rich and polymer-rich phases. Depending on the population, composition, and location of each phase, the consequences of dissolution performance can vary. If the dissolving front is not blocked by drug-rich phases, for ASDs at drug loadings above the congruent release boundary, the fast-releasing polymer-rich phases formed can improve ASD dissolution performance.[15] Particle size reduction resulting from the formation of submicron heterogeneous domains may also promote drug release rate.[72,73] For ASDs at drug loadings below or equal to the congruent release boundary, the formation of drug-rich phases can reduce the amount of drug available for fast release (due to the reduced population of low-drug-loading phases) and thus lead to compromised drug release rates. If the dissolving front is covered by slow-releasing drug-rich phases, a decline in drug release rate is also likely to occur.[15] Such surface drug enrichment-induced slow release has been previously observed for ASDs in spray-dried particles, tablets, and film systems.[15,31,67]

In this study, the surface composition of SDDs at a 25% drug loading varied with spray solvent composition. More water added in the solvent system resulted in higher drug content on the surface as observed by XPS and fluorescence spectra. For these systems, lower drug release was observed as compared to the miscible ASD, likely due to surface drug enrichment and the reduction in the amount of drug available for congruent release. Overall, faster drug release was achieved at a 25% drug loading in all samples regardless of spray solvent composition and when compared to higher-drug-loading ASDs, and solution drug concentrations exceeded the amorphous solubility boundary in both miscible and phase-separated systems (Table 4). The 50 and 75% drug loading systems showed drug release rates slightly higher or similar to

that of neat amorphous ritonavir (Figure 9). Although compositional differences were observed in phase-separated ASDs on the surface (varying from 38 to 91% ritonavir; Figure 7), the drug concentrations appeared to be well above the congruent release boundary of the system and therefore incongruent-type release kinetics was observed, with drug release rates being similar to that of the neat amorphous drug. Therefore, the impact of phase separation on ASD dissolution, either promoting or compromising drug release, is expected to be more profound in low-drug-loading systems, where the drug release is congruent or close to congruent to that of the polymer.

Compared to the solid-state characterization techniques used in this study, the release test showed the highest sensitivity to subtle differences in SDD homogeneity for the low-drug-loading systems. DSC with carefully designed sample preparation procedures can also provide useful information about subtle microstructural changes. Although powerful analytical techniques with higher sensitivity for direct miscibility characterization may be needed, routine dissolution tests and DSC runs can serve as quality indicators.

■ CONCLUSIONS

Water addition to the solvent system can lead to phase separation of amorphous solid dispersions during spray drying even for an initially one-phase stock solution. For the ritonavir−PVPVA system investigated herein, at a 25% drug loading with a 10:90 H_2O/MeOH solvent ratio, such phase separation appeared to be subtle and was hard to capture using a variety of solid-state characterization techniques, although a significant reduction in drug release rate was noted. Both experimental and modeling results suggested that the extent of phase separation increases with a higher amount of water added to the spray solvent. For the same solvent composition, high-drug-loading ASDs are more prone to phase separation during spray drying than low-drug-loading systems, but the impact of phase separation on drug release rates may be minimal in these systems, due to the already compromised release often seen at high drug loadings. These findings regarding solvent composition and its impact on spray-dried amorphous solid dispersions are expected to aid in the rational design of spray drying processing conditions and can broadly contribute to the risk assessment of other solvent-based process using mixed organic solvents.

■ ASSOCIATED CONTENT

ⓢ Supporting Information

The Supporting Information is available free of charge at https://pubs.acs.org/doi/10.1021/acs.molpharmaceut.0c00798.

Surface drug distribution in SDDs from XPS analysis (Table S1) and droplet drying model incorporating a four-component thermodynamic phase model (PDF)

■ AUTHOR INFORMATION

Corresponding Author

Lynne S. Taylor − *Department of Industrial and Physical Pharmacy, Purdue University, West Lafayette, Indiana 47907, United States;* ⓞ orcid.org/0000-0002-4568-6021; Email: lstaylor@purdue.edu

Authors

Na Li − *Department of Industrial and Physical Pharmacy, Purdue University, West Lafayette, Indiana 47907, United States; Department of Pharmaceutical Sciences, University of Connecticut, Storrs, Connecticut 06269, United States*

Jonathan L. Cape − *Research & Development, Lonza Pharma and Biotech, Bend, Oregon 97703, United States*

Bharat R. Mankani − *Department of Industrial and Physical Pharmacy, Purdue University, West Lafayette, Indiana 47907, United States; MarqMetrix Inc., Seattle, Washington 98103, United States*

Dmitry Y. Zemlyanov − *Birck Nanotechnology Center, Purdue University, West Lafayette, Indiana 47907, United States;* ⊙ orcid.org/0000-0002-1221-9195

Kimberly B. Shepard − *Research & Development, Lonza Pharma and Biotech, Bend, Oregon 97703, United States*

Michael M. Morgen − *Research & Development, Lonza Pharma and Biotech, Bend, Oregon 97703, United States*

Complete contact information is available at:
https://pubs.acs.org/10.1021/acs.molpharmaceut.0c00798

Notes

The authors declare no competing financial interest.

■ ABBREVIATIONS USED

AFM, atomic force microscopy; ASD, amorphous solid dispersion; DSC, differential scanning calorimetry; HPLC, high-performance liquid chromatography; PVPVA, poly-(vinylpyrrolidone-co-vinyl acetate); PXRD, powder X-ray diffraction; RTV, ritonavir; SNDR, surface-normalized dissolution rate; SDD, spray-dried dispersion; ssNMR, solid-state nuclear magnetic resonance spectroscopy; TEM, transmission electron microscopy; XPS, X-ray photoelectron spectroscopy

■ REFERENCES

(1) Lipinski, C. A. Drug-like properties and the causes of poor solubility and poor permeability. *J. Pharmacol. Toxicol. Methods* **2000**, *44*, 235−249.

(2) Di, L.; Fish, P. V.; Mano, T. Bridging solubility between drug discovery and development. *Drug Discovery Today* **2012**, *17*, 486−495.

(3) Chen, H.; Pui, Y.; Liu, C.; Chen, Z.; Su, C.-C.; Hageman, M.; Hussain, M.; Haskell, R.; Stefanski, K.; Foster, K.; Gudmundsson, O.; Qian, F. Moisture-Induced Amorphous Phase Separation of Amorphous Solid Dispersions: Molecular Mechanism, Microstructure, and Its Impact on Dissolution Performance. *J. Pharm. Sci.* **2018**, *107*, 317−326.

(4) Dahan, A.; Beig, A.; Lindley, D.; Miller, J. M. The solubility−permeability interplay and oral drug formulation design: Two heads are better than one. *Adv. Drug Delivery Rev.* **2016**, *101*, 99−107.

(5) Miller, J. M.; Beig, A.; Carr, R. A.; Spence, J. K.; Dahan, A. A Win−Win Solution in Oral Delivery of Lipophilic Drugs: Super-saturation via Amorphous Solid Dispersions Increases Apparent Solubility without Sacrifice of Intestinal Membrane Permeability. *Mol. Pharmaceutics* **2012**, *9*, 2009−2016.

(6) Fischer, S. M.; Flaten, G. E.; Hagesæther, E.; Fricker, G.; Brandl, M. In-vitro permeability of poorly water soluble drugs in the phospholipid vesicle-based permeation assay: the influence of nonionic surfactants. *J. Pharm. Pharmacol.* **2011**, *63*, 1022−1030.

(7) Raina, S.; Zhang, G. Z.; Alonzo, D.; Wu, J.; Zhu, D.; Catron, N.; Gao, Y.; Taylor, L. Impact of solubilizing additives on supersaturation and membrane transport of drugs. *Pharm. Res.* **2015**, 3350−3364.

(8) Mugheirbi, N. A.; Marsac, P. J.; Taylor, L. S. Insights into Water-Induced Phase Separation in Itraconazole−Hydroxypropylmethyl Cellulose Spin Coated and Spray Dried Dispersions. *Mol. Pharmaceutics* **2017**, *14*, 4387−4402.

(9) Chen, Z.; Yang, K.; Huang, C.; Zhu, A.; Yu, L.; Qian, F. Surface Enrichment and Depletion of the Active Ingredient in Spray Dried Amorphous Solid Dispersions. *Pharm. Res.* **2018**, *35*, No. 38.

(10) Rumondor, A. F.; Wikström, H.; Van Eerdenbrugh, B.; Taylor, L. Understanding the Tendency of Amorphous Solid Dispersions to Undergo Amorphous−Amorphous Phase Separation in the Presence of Absorbed Moisture. *AAPS PharmSciTech* **2011**, *12*, 1209−1219.

(11) Qian, F.; Huang, J.; Zhu, Q.; Haddadin, R.; Gawel, J.; Garmise, R.; Hussain, M. Is a distinctive single Tg a reliable indicator for the homogeneity of amorphous solid dispersion? *Int. J. Pharm.* **2010**, *395*, 232−235.

(12) Purohit, H. S.; Taylor, L. S. Phase Behavior of Ritonavir Amorphous Solid Dispersions during Hydration and Dissolution. *Pharm. Res.* **2017**, *34*, 2842−2861.

(13) Rumondor, A. F.; Stanford, L.; Taylor, L. Effects of Polymer Type and Storage Relative Humidity on the Kinetics of Felodipine Crystallization from Amorphous Solid Dispersions. *Pharm. Res.* **2009**, *26*, 2599−2606.

(14) Marsac, P. J.; Rumondor, A. C. F.; Nivens, D. E.; Kestur, U. S.; Stanciu, L.; Taylor, L. S. Effect of temperature and moisture on the miscibility of amorphous dispersions of felodipine and poly(vinyl pyrrolidone). *J. Pharm. Sci.* **2010**, *99*, 169−185.

(15) Li, N.; Taylor, L. S. Microstructure Formation for Improved Dissolution Performance of Lopinavir Amorphous Solid Dispersions. *Mol. Pharmaceutics* **2019**, *16*, 1751−1765.

(16) Baird, J. A.; Van Eerdenbrugh, B.; Taylor, L. S. A classification system to assess the crystallization tendency of organic molecules from undercooled melts. *J. Pharm. Sci.* **2010**, *99*, 3787−3806.

(17) Qi, S.; Moffat, J. G.; Yang, Z. Early Stage Phase Separation in Pharmaceutical Solid Dispersion Thin Films under High Humidity: Improved Spatial Understanding Using Probe-Based Thermal and Spectroscopic Nanocharacterization Methods. *Mol. Pharmaceutics* **2013**, *10*, 918−930.

(18) Li, N.; Taylor, L. S. Nanoscale Infrared, Thermal, and Mechanical Characterization of Telaprevir−Polymer Miscibility in Amorphous Solid Dispersions Prepared by Solvent Evaporation. *Mol. Pharmaceutics* **2016**, *13*, 1123−1136.

(19) Ricarte, R. G.; Lodge, T. P.; Hillmyer, M. A. Nanoscale Concentration Quantification of Pharmaceutical Actives in Amorphous Polymer Matrices by Electron Energy-Loss Spectroscopy. *Langmuir* **2016**, *32*, 7411−7419.

(20) Van Eerdenbrugh, B.; Lo, M.; Kjoller, K.; Marcott, C.; Taylor, L. S. Nanoscale mid-infrared imaging of phase separation in a drug−polymer blend. *J. Pharm. Sci.* **2012**, *101*, 2066−2073.

(21) Purohit, H. S.; Taylor, L. S. Miscibility of Itraconazole-Hydroxypropyl Methylcellulose Blends- Insights with High Resolution Analytical Methodologies. *Mol. Pharmaceutics* **2015**, *12*, 4542−4553.

(22) Saboo, S.; Taylor, L. S. Water-induced phase separation of miconazole-poly (vinylpyrrolidone-co-vinyl acetate) amorphous solid dispersions: Insights with confocal fluorescence microscopy. *Int. J. Pharm.* **2017**, *529*, 654−666.

(23) Li, N.; Gilpin, C. J.; Taylor, L. S. Understanding the Impact of Water on the Miscibility and Microstructure of Amorphous Solid Dispersions: An AFM−LCR and TEM−EDX Study. *Mol. Pharmaceutics* **2017**, *14*, 1691−1705.

(24) Qi, S.; Belton, P.; Nollenberger, K.; Gryczke, A.; Craig, D. M. Compositional Analysis of Low Quantities of Phase Separation in Hot-Melt-Extruded Solid Dispersions: A Combined Atomic Force Microscopy, Photothermal Fourier-Transform Infrared Microspectroscopy, and Localised Thermal Analysis Approach. *Pharm. Res.* **2011**, *28*, 2311−2326.

(25) Purohit, H. S.; Ormes, J. D.; Saboo, S.; Su, Y.; Lamm, M. S.; Mann, A. K. P.; Taylor, L. S. Insights into Nano- and Micron-Scale Phase Separation in Amorphous Solid Dispersions Using Fluorescence-Based Techniques in Combination with Solid State Nuclear Magnetic Resonance Spectroscopy. *Pharm. Res.* **2017**, 1364−1377.

(26) Calahan, J. L.; Zanon, R. L.; Alvarez-Nunez, F.; Munson, E. J. Isothermal Microcalorimetry To Investigate the Phase Separation for Amorphous Solid Dispersions of AMG 517 with HPMC-AS. *Mol. Pharmaceutics* **2013**, *10*, 1949−1957.

(27) Sarpal, K. Phase Behavior of Amorphous Solid Dispersions: Miscibility and Molecular Interactions. PhD Dissertation, University of Kentucky, 2019.

(28) Yuan, X.; Sperger, D.; Munson, E. J. Investigating Miscibility and Molecular Mobility of Nifedipine-PVP Amorphous Solid Dispersions Using Solid-State NMR Spectroscopy. *Mol. Pharmaceutics* **2014**, *11*, 329−337.

(29) Purohit, H. S.; Taylor, L. S. Phase Separation Kinetics in Amorphous Solid Dispersions Upon Exposure to Water. *Mol. Pharmaceutics* **2015**, *12*, 1623−1635.

(30) Tian, B.; Tang, X.; Taylor, L. S. Investigating the Correlation between Miscibility and Physical Stability of Amorphous Solid Dispersions Using Fluorescence-Based Techniques. *Mol. Pharmaceutics* **2016**, *13*, 3988−4000.

(31) Bhardwaj, V.; Trasi, N. S.; Zemlyanov, D. Y.; Taylor, L. S. Surface area normalized dissolution to study differences in itraconazole-copovidone solid dispersions prepared by spray-drying and hot melt extrusion. *Int. J. Pharm.* **2018**, *540*, 106−119.

(32) Bhujbal, S. V.; Zemlyanov, D. Y.; Cavallaro, A.; Mangal, S.; Taylor, L. S.; Zhou, Q. T. Qualitative and Quantitative Characterization of Composition Heterogeneity on the Surface of Spray Dried Amorphous Solid Dispersion Particles by an Advanced Surface Analysis Platform with High Surface Sensitivity and Superior Spatial Resolution. *Mol. Pharmaceutics* **2018**, *15*, 2045−2053.

(33) Huang, Y.; Dai, W.-G. Fundamental aspects of solid dispersion technology for poorly soluble drugs. *Acta Pharm. Sin. B* **2014**, *4*, 18−25.

(34) Marsac, P.; Shamblin, S.; Taylor, L. Theoretical and Practical Approaches for Prediction of Drug−Polymer Miscibility and Solubility. *Pharm. Res.* **2006**, *23*, 2417−2426.

(35) Meng, F.; Trivino, A.; Prasad, D.; Chauhan, H. Investigation and correlation of drug polymer miscibility and molecular interactions by various approaches for the preparation of amorphous solid dispersions. *Eur. J. Pharm. Sci.* **2015**, *71*, 12−24.

(36) Thakral, S.; Thakral, N. K. Prediction of drug−polymer miscibility through the use of solubility parameter based flory−huggins interaction parameter and the experimental validation: PEG as model polymer. *J. Pharm. Sci.* **2013**, *102*, 2254−2263.

(37) Prudic, A.; Ji, Y.; Sadowski, G. Thermodynamic Phase Behavior of API/Polymer Solid Dispersions. *Mol. Pharmaceutics* **2014**, *11*, 2294−2304.

(38) Vasanthavada, M.; Tong, W.-Q.; Joshi, Y.; Kislalioglu, M. S. Phase Behavior of Amorphous Molecular Dispersions I: Determination of the Degree and Mechanism of Solid Solubility. *Pharm. Res.* **2004**, *21*, 1598−1606.

(39) Paudel, A.; Van Humbeeck, J.; Van den Mooter, G. Theoretical and Experimental Investigation on the Solid Solubility and Miscibility of Naproxen in Poly(vinylpyrrolidone). *Mol. Pharmaceutics* **2010**, *7*, 1133−1148.

(40) Janssens, S.; De Zeure, A.; Paudel, A.; Van Humbeeck, J.; Rombaut, P.; Van den Mooter, G. Influence of Preparation Methods on Solid State Supersaturation of Amorphous Solid Dispersions: A Case Study with Itraconazole and Eudragit E100. *Pharm. Res.* **2010**, *27*, 775−785.

(41) Parikh, T.; Gupta, S. S.; Meena, A. K.; Vitez, I.; Mahajan, N.; Serajuddin, A. T. M. Application of Film-Casting Technique to Investigate Drug−Polymer Miscibility in Solid Dispersion and Hot-Melt Extrudate. *J. Pharm. Sci.* **2015**, *104*, 2142−2152.

(42) Qi, S.; Belton, P.; Nollenberger, K.; Clayden, N.; Reading, M.; Craig, D. Q. M. Characterisation and Prediction of Phase Separation in Hot-Melt Extruded Solid Dispersions: A Thermal, Microscopic and NMR Relaxometry Study. *Pharm. Res.* **2010**, *27*, 1869−1883.

(43) Lauer, M.; Siam, M.; Tardio, J.; Page, S.; Kindt, J.; Grassmann, O. Rapid Assessment of Homogeneity and Stability of Amorphous Solid Dispersions by Atomic Force Microscopy—From Bench to Batch. *Pharm. Res.* **2013**, *30*, 2010−2022.

(44) Abu-Diak, O. A.; Jones, D. S.; Andrews, G. P. Understanding the performance of melt-extruded poly(ethylene oxide)−bicalutamide solid dispersions: Characterisation of microstructural properties using thermal, spectroscopic and drug release methods. *J. Pharm. Sci.* **2012**, *101*, 200−213.

(45) Paudel, A.; Van den Mooter, G. Influence of Solvent Composition on the Miscibility and Physical Stability of Naproxen/PVP K 25 Solid Dispersions Prepared by Cosolvent Spray-Drying. *Pharm. Res.* **2012**, *29*, 251−270.

(46) Al-Obaidi, H.; Brocchini, S.; Buckton, G. Anomalous properties of spray dried solid dispersions. *J. Pharm. Sci.* **2009**, *98*, 4724−4737.

(47) Worku, Z. A.; Aarts, J.; Singh, A.; Van den Mooter, G. Drug−Polymer Miscibility across a Spray Dryer: A Case Study of Naproxen and Miconazole Solid Dispersions. *Mol. Pharmaceutics* **2014**, *11*, 1094−1101.

(48) Thompson, J. W.; Kaiser, T. J.; Jorgenson, J. W. Viscosity measurements of methanol−water and acetonitrile−water mixtures at pressures up to 3500bar using a novel capillary time-of-flight viscometer. *J. Chromatogr. A* **2006**, *1134*, 201−209.

(49) Herráez, J. V.; Belda, R. Refractive Indices, Densities and Excess Molar Volumes of Monoalcohols + Water. *J. Solution Chem.* **2006**, *35*, 1315−1328.

(50) BASF Kollidon VA 64: Technical Information. https://www.stobec.com/DATA/PRODUIT/2289~v~fiche-technique.pdf.

(51) Law, D.; Krill, S. L.; Schmitt, E. A.; Fort, J. J.; Qiu, Y.; Wang, W.; Porter, W. R. Physicochemical considerations in the preparation of amorphous ritonavir-poly(ethylene glycol) 8000 solid dispersions. *J. Pharm. Sci.* **2001**, *90*, 1015−1025.

(52) Law, D.; Schmitt, E. A.; Marsh, K. C.; Everitt, E. A.; Wang, W.; Fort, J. J.; Krill, S. L.; Qiu, Y. Ritonavir-PEG 8000 amorphous solid dispersions: in vitro and in vivo evaluations. *J. Pharm. Sci.* **2004**, *93*, 563−570.

(53) Ilevbare, G. A.; Taylor, L. S. Liquid−Liquid Phase Separation in Highly Supersaturated Aqueous Solutions of Poorly Water-Soluble Drugs: Implications for Solubility Enhancing Formulations. *Cryst. Growth Des.* **2013**, *13*, 1497−1509.

(54) Bains, G. K.; Kim, S. H.; Sorin, E. J.; Narayanaswami, V. The Extent of Pyrene Excimer Fluorescence Emission Is a Reflector of Distance and Flexibility: Analysis of the Segment Linking the LDL Receptor-Binding and Tetramerization Domains of Apolipoprotein E3. *Biochemistry* **2012**, *51*, 6207−6219.

(55) Mosquera-Giraldo, L. I.; Li, N.; Wilson, V. R.; Nichols, B. L. B.; Edgar, K. J.; Taylor, L. S. Influence of Polymer and Drug Loading on the Release Profile and Membrane Transport of Telaprevir. *Mol. Pharmaceutics* **2018**, *15*, 1700−1713.

(56) Ueda, K.; Taylor, L. S. Polymer Type Impacts Amorphous Solubility and Drug-Rich Phase Colloidal Stability: A Mechanistic Study Using Nuclear Magnetic Resonance Spectroscopy. *Mol. Pharmaceutics* **2020**, *17*, 1352−1362.

(57) Sun, D. D.; Wen, H.; Taylor, L. S. Non-Sink Dissolution Conditions for Predicting Product Quality and In Vivo Performance of Supersaturating Drug Delivery Systems. *J. Pharm. Sci.* **2016**, 2477−2488.

(58) Jog, R.; Burgess, D. J. Nanoamorphous drug products − Design and development. *Int. J. Pharm.* **2018**, *553*, 238−260.

(59) Baird, J. A.; Taylor, L. S. Evaluation of amorphous solid dispersion properties using thermal analysis techniques. *Adv. Drug Delivery Rev.* **2012**, *64*, 396−421.

(60) Gaikwad, A. N.; Wood, E. R.; Ngai, T.; Lodge, T. P. Two Calorimetric Glass Transitions in Miscible Blends Containing Poly(ethylene oxide). *Macromolecules* **2008**, *41*, 2502−2508.

(61) Miwa, Y.; Usami, K.; Yamamoto, K.; Sakaguchi, M.; Sakai, M.; Shimada, S. Direct Detection of Effective Glass Transitions in

Miscible Polymer Blends by Temperature-Modulated Differential Scanning Calorimetry. *Macromolecules* **2005**, *38*, 2355−2361.

(62) Sakaguchi, T.; Taniguchi, N.; Urakawa, O.; Adachi, K. Calorimetric Study of Dynamical Heterogeneity in Blends of Polyisoprene and Poly(vinylethylene). *Macromolecules* **2005**, *38*, 422−428.

(63) de Andrade, M. L.; Atvars, T. D. Z. Dynamic and Static Fluorescence Spectroscopy Applied to Miscibility of Poly(n-butyl methacrylate-co-styrene) with Polystyrene and Morphological Analysis by Epifluorescence Microscopy. *J. Phys. Chem. B* **2004**, *108*, 3975−3984.

(64) Huang, J.; Chen, P. X.; Wettig, S. Fluorescence-based techniques to assess the miscibility and physical stability of a drug−lipid complex. *Can. J. Chem.* **2019**, *97*, 496−503.

(65) Evans, C. M.; Torkelson, J. M. Determining multiple component glass transition temperatures in miscible polymer blends: Comparison of fluorescence spectroscopy and differential scanning calorimetry. *Polymer* **2012**, *53*, 6118−6124.

(66) Kalyanasundaram, K.; Thomas, J. K. Environmental effects on vibronic band intensities in pyrene monomer fluorescence and their application in studies of micellar systems. *J. Am. Chem. Soc.* **1977**, *99*, 2039−2044.

(67) Indulkar, A. S.; Lou, X.; Zhang, G. G. Z.; Taylor, L. S. Insights into the Dissolution Mechanism of Ritonavir−Copovidone Amorphous Solid Dispersions: Importance of Congruent Release for Enhanced Performance. *Mol. Pharmaceutics* **2019**, *16*, 1327−1339.

(68) Saboo, S.; Mugheirbi, N. A.; Zemlyanov, D. Y.; Kestur, U. S.; Taylor, L. S. Congruent release of drug and polymer: A "sweet spot" in the dissolution of amorphous solid dispersions. *J. Controlled Release* **2019**, *298*, 68−82.

(69) Saboo, S.; Kestur, U. S.; Flaherty, D. P.; Taylor, L. S. Congruent Release of Drug and Polymer from Amorphous Solid Dispersions: Insights into the Role of Drug-Polymer Hydrogen Bonding, Surface Crystallization, and Glass Transition. *Mol. Pharmaceutics* **2020**, *17*, 1261−1275.

(70) Que, C.; Lou, X.; Zemlyanov, D. Y.; Mo, H.; Indulkar, A. S.; Gao, Y.; Zhang, G. G. Z.; Taylor, L. S. Insights into the Dissolution Behavior of Ledipasvir−Copovidone Amorphous Solid Dispersions: Role of Drug Loading and Intermolecular Interactions. *Mol. Pharmaceutics* **2019**, *16*, 5054−5067.

(71) Simonelli, A. P.; Mehta, S. C.; Higuchi, W. I. Dissolution Rates of High Energy Polyvinylpyrrolidone (PVP)-Sulfathiazole Coprecipitates. *J. Pharm. Sci.* **1969**, *58*, 538−549.

(72) Matteucci, M. E.; Brettmann, B. K.; Rogers, T. L.; Elder, E. J.; Williams, R. O.; Johnston, K. P. Design of Potent Amorphous Drug Nanoparticles for Rapid Generation of Highly Supersaturated Media. *Mol. Pharmaceutics* **2007**, *4*, 782−793.

(73) Sjökvist, E.; Nyström, C. Physicochemical aspects of drug release. VI. Drug dissolution rate from solid particulate dispersions and the importance of carrier and drug particle properties. *Int. J. Pharm.* **1988**, *47*, 51−66.